Electronic Supplementary Material (ESI) for Inorganic Chemistry Frontiers.

Supporting Information

A novel red-emitting phosphor with an unusual concentration quenching effect for near-UV based WLEDs

Nan Yang, [a] Ziwang Zhang, [a] Liyuan Zou, [a] Jun Chen, [a] Haiyong Ni, [b] Pin Chen, [c] Jianxin Shi, *[a] and Yexiang Tong [a,d]

[a] *School of Chemistry, Sun Yat-Sen University, Guangzhou 510006, P. R. China.*

[b] *Guangdong Province Key Laboratory of Rare Earth Development and Application, Institute of Resources Utilization and Rare Earth Development, Guangdong Academy of Sciences, Guangzhou 510651, P. R. China.*

[c] *National Supercomputer Center in Guangzhou, School of Computer Science and Engineering, Sun Yat-Sen University, Guangzhou 510006, P. R. China.*

[d] *MOE of the Key Laboratory of Bioinorganic and Synthetic Chemistry, The Key Lab of Low-Carbon Chemistry & Energy Conservation of Guangdong Province, Sun Yat-sen University, Guangzhou 510006, P. R. China.*

* Corresponding author: cessjx@mail.sysu.edu.cn

Table of Contents

Remark: The sequence of the table of contents is consistent with the order of the relevant content appearing in the manuscript.

Table S1 The metal atomic parameters including oxidation number (Ox.), Wyckoff symbol (Wyck.) and site occupation fraction (S.O.F.) of the simplified ordered structure of GGTO.

Atoms	Ox.	Wyck.	S.O.F.
Gd1	3	8d	1
Ti1	4	8d	1
Ga2	3	4c	1
Ti3	4	8d	1
Ga4	3	4c	1

There are many disorder atoms of Ga and Ti existing in GGTO (details shown in section 3.1 in the manuscript), which brings great difficulties for building models, therefore, a simplified ordered structure is proposed based on the following assumptions:

(1) The co-occupied sites by Ga1 and Ti1 are assumed as only occupied by Ti;

(2) The co-occupied sites by Ga2 and Ti2 are assumed as only occupied by Ga;

(3) The co-occupied sites by Ga3 and Ti3 are assumed as only occupied by Ti;

(4) The site occupation fraction (S.O.F.) of both Ga4 is assumed to be 1 while that of Ga5 is 0.

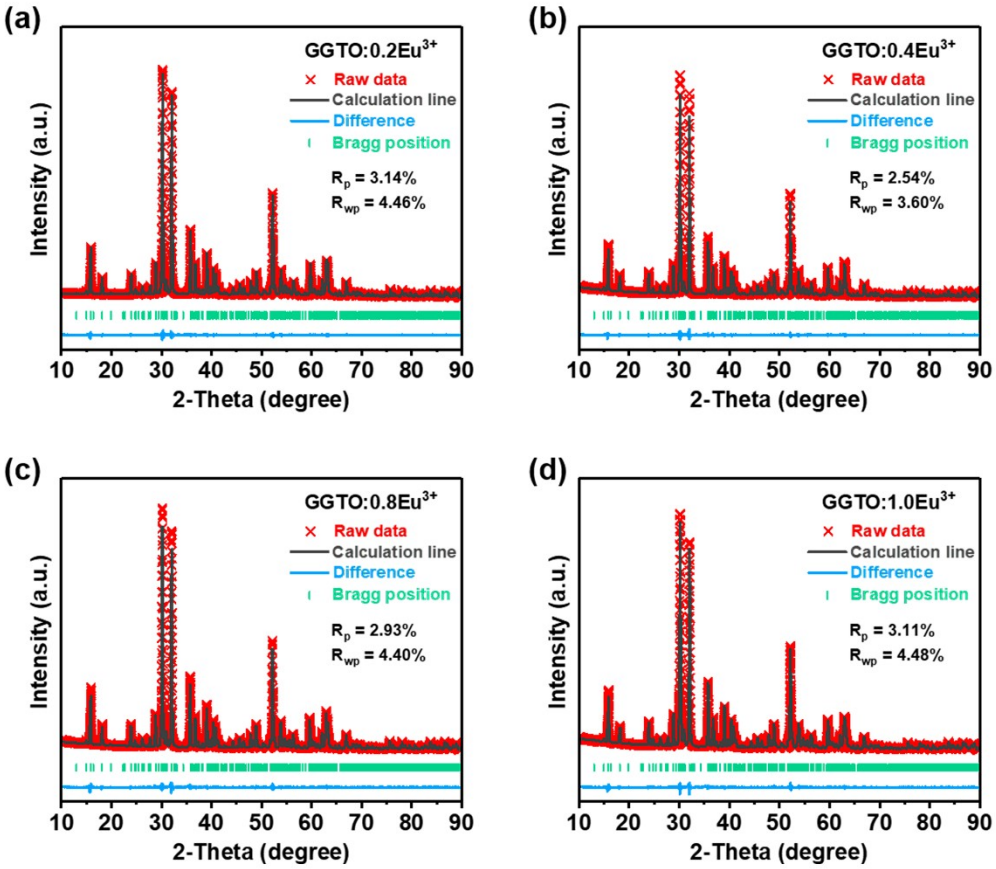

Fig. S1 The refinement profiles of GGTO:xEu^{3+} (x = 0.2, 0.4, 0.8, and 1.0).

Table S2 The refined structural parameters for GGTO:*x*Eu^{3+} (*x* = 0.2, 0.4, 0.6, 0.8, 1.0).

GGTO:*x*Eu^{3+}	**0.2**	**0.4**	**0.6**	**0.8**	**1.0**
GOF	2.30	2.09	2.44	2.54	2.39
R_p (%)	3.14	2.54	2.89	2.93	3.11
R_{wp} (%)	4.46	3.60	4.21	4.40	4.48
a (Å)	9.7922	9.7927	9.7923	9.7933	9.7977
b (Å)	13.6218	13.6243	13.6260	13.6309	13.6362
c (Å)	7.4424	7.4466	7.4490	7.4567	7.4578
V ($Å^3$)	992.72	993.51	993.92	995.41	996.38

Table S2 shows the refinement data and the cell parameters of the GGTO:*x*Eu^{3+} (*x* = 0.2, 0.4, 0.6, 0.8, 1.0). The goodness-of-fit parameters of all the samples are small enough, especially the final reliability factors (R_p and R_{wp}) of the representative sample, GGTO:0.6Eu^{3+}, are 2.89% and 4.21%, respectively, indicating that the introduction of Eu^{3+} does not produce any phase impurity in GGTO. Additionally, the unit cell volume of GGTO:*x*Eu^{3+} increases gradually with increasing the doping concentration of Eu^{3+}, which is the result of the substitution of smaller ions (Gd^{3+}) by larger dopant ions (Eu^{3+}).

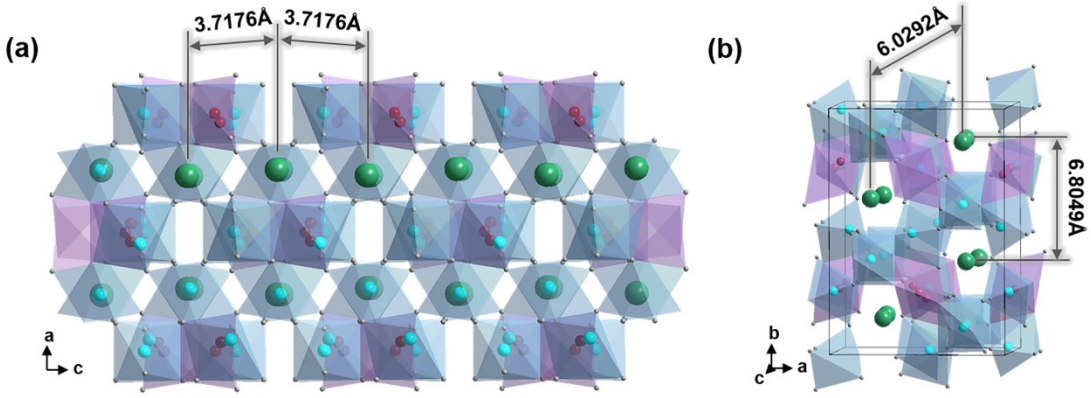

Fig. S2 The chain structure of GGTO viewing from *b* axis (a) and *c* axis (b).

Table S3 The atomic and weight percentages of GGTO:0.6Eu^{3+} in the EDS elemental mappings.

GGTO:0.6Eu^{3+}	Atomic (%)	Weight (%)
Ga	7.58	14.67
Gd	3.26	14.25
Ti	14.46	19.22
O	69.74	30.97
Eu	4.95	20.89

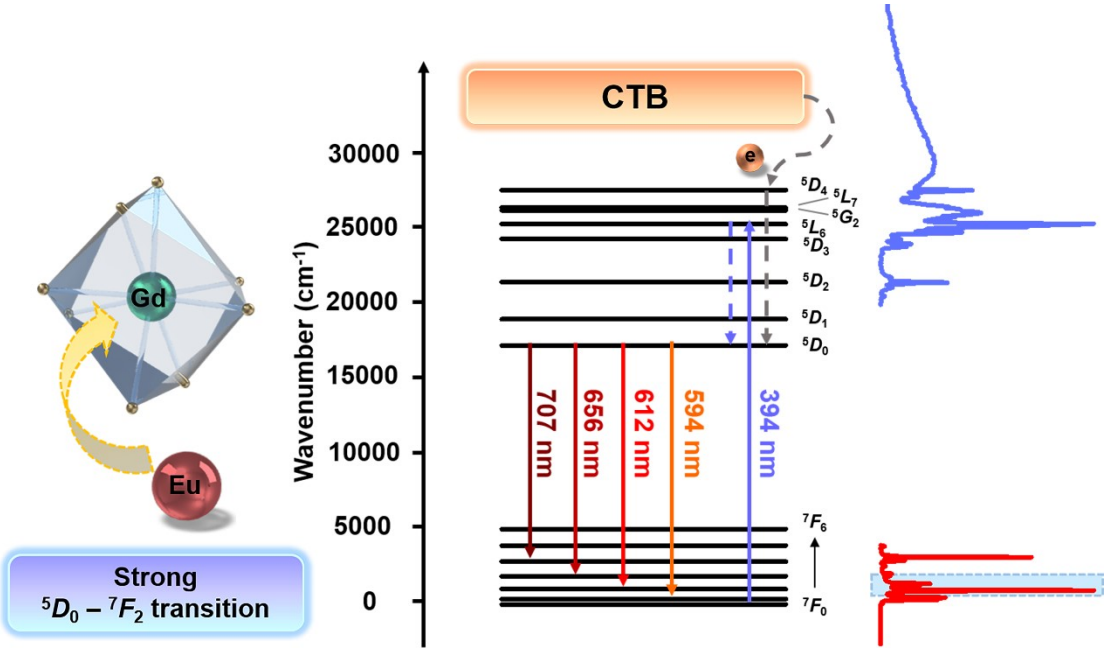

Fig. S3 The scheme of energy levels for GGTO:Eu^{3+}.

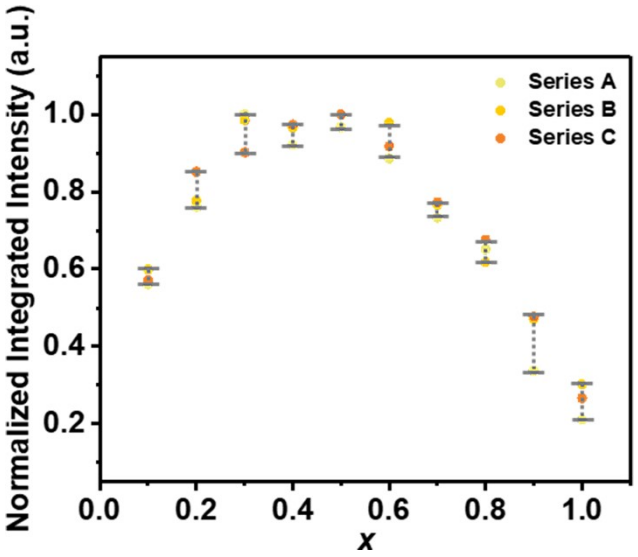

Fig. S4 The changing trend of the integrated emission intensity excited at 394 nm and the deviation area of three parallel experiments GGTO:xEu^{3+}.

Table S4. CIE chromaticity coordinates and colour purity of GGTO:*x*Eu^{3+}

GGTO:*x*Eu^{3+}	CIE (*x*, *y*)	Colour purity (%)
0.1	（0.6403，0.3562）	91.9
0.2	(0.6433，0.3548)	92.7
0.3	（0.6447，0.3537）	93.0
0.4	(0.6455，0.3531)	93.2
0.5	（0.6462，0.3527）	93.4
0.6	(0.6466，0.3523)	93.5
0.7	（0.6467，0.3522）	93.5
0.8	(0.6466，0.3519)	93.5
0.9	（0.6465，0.3520）	93.5
1.0	(0.6465，0.3516)	93.4

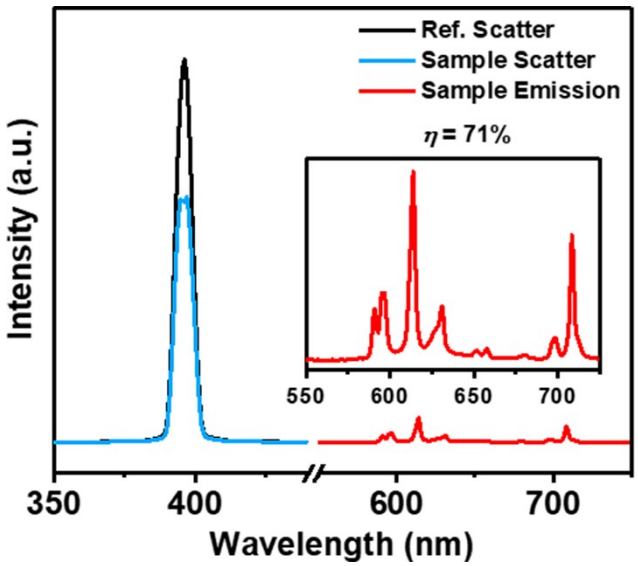

Fig. S5 Quantum efficiency of GGTO:0.6Eu^{3+}.

Table S5. Quantum efficiency (η) of GGTO:xEu^{3+}

GGTO:xEu^{3+}	η **(%)**
0.1	44.9
0.2	59.2
0.3	70.5
0.4	69.5
0.5	66.8
0.6	70.8
0.7	50.7
0.8	40.3
0.9	26.7
1.0	17.5

Table S6. Judd-Ofelt studies on the photoluminescence data of the GGTO:*x*Eu^{3+} phosphors.

GGTO:*x*Eu^{3+}	I_{01}	I_{02}	I_{02}/I_{01}	A_{02} (s^{-1})	Ω_2 (×10^{-20} cm^2)
0.1	16474200	37520800	2.28	117.33	3.82
0.2	21258300	49337700	2.32	119.56	3.90
0.3	26662200	63014800	2.36	121.75	3.97
0.4	25800500	61815900	2.40	123.43	4.02
0.5	26696800	64446400	2.41	124.36	4.05
0.6	25941400	63246100	2.44	125.60	4.09
0.7	20302100	49557700	2.44	125.75	4.10
0.8	16318200	39991400	2.45	126.25	4.11
0.9	12346700	30227100	2.45	126.12	4.11
1.0	7866940	19541000	2.48	127.96	4.17

The local structure environment around the Eu^{3+} ions in GGTO host can be analysed by calculating the radiative transition rates (A) and the intensity parameters Ω_λ (λ = 2, 4, 6) based on the Judd-Ofelt theory. The integrated emission intensity of the $^5D_0$ - ^7F_J (J = 0, 1, 2, 3, 4) transitions can be defined as:[1,2]

$$I_{i-j} = \hbar\omega_{i-j} A_{i-j} N_i \# \quad (1)$$

where i and j refer to the initial ($^5D_0$) and final levels ($^7F_{0\text{-}4}$), respectively, $\hbar\omega_{i-j}$ refers to the transition energy, A_{i-j} refers to the Einstein's coefficient of spontaneous emission, and N_i refers to the population of the $^5D_0$ excited state. The magnetic dipole transition of $^5D_0$ - $^7F_1$ is relatively insensitive to the local environment around Eu^{3+} ions, and so it is much suitable for reference. The radiative transition rates A_{0J} $(J = 2, 3, 4)$ can be obtained by the following equation:[3]

$$A_{0J} = A_{01}\left(\frac{I_{0J}}{I_{01}}\right)\left(\frac{v_{01}}{v_{0J}}\right) \# \quad (2)$$

where I_{01} and I_{0J} are the integral intensity of the transitions $^5D_0$ - $^7F_1$ and $^5D_0$ - ^7F_J, respectively, v_{01} and v_{0J} are wavenumbers of the corresponding transitions, respectively.

According to the Judd-Ofelt theory, the radiative transition rate of the electric dipole transitions of $^5D_0$ - ^7F_J (J = 2, 4, 6) is defined as follows:[2,4]

$$A_{J-J'}^{ED} = \frac{64\pi^4 v^3 e^2}{3h(2J+1)} \frac{n(n^2+2)^2}{9} \sum_{\lambda=2,4,6} \Omega_\lambda \left| \langle \psi J \| U^{(\lambda)} \| \psi' J' \rangle \right|^2 \# \quad (3)$$

where v is the center wavenumber of ED transitions, e is elementary charge (4.8 ×10^{-10} esu), h refers to Planck coefficient and the value is 6.626 × 10^{-27} erg s, n refers to the refractive index, and $\langle \psi J \| U^{(\lambda)} \| \psi' J' \rangle^2$ refers to the reduced matrix element for the $J-J'$ electric dipole transitions, whose values are 0.0032, 0.0023 and 0.0002 corresponding to λ of 2, 4 and 6, respectively. As known that $(A_{01})_{vac}$ is 14.65 s^{-1} in vacuo and an average index of refraction n is 1.506, the value of A_{01} is estimated to be 50 s^{-1} in air from the equation of $A_{01} = n^3 (A_{01})_{vac}$.[1-3]

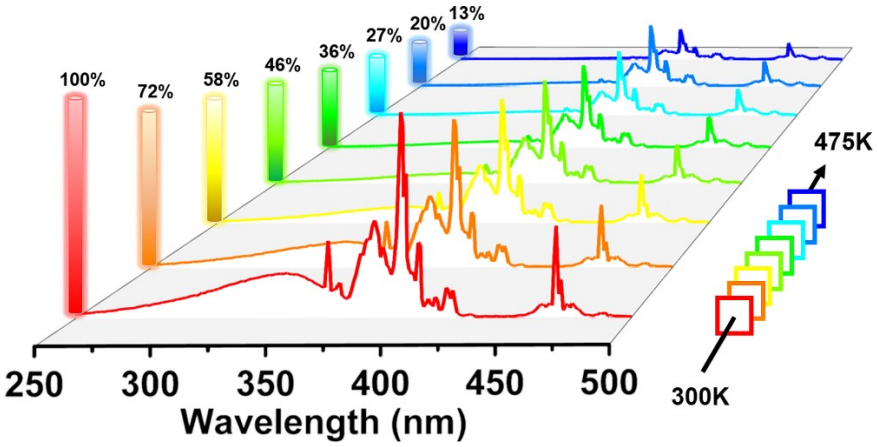

Fig. S6 The temperature-dependent excitation spectra of GGTO:0.6Eu^{3+}.

Table S7. CIE chromaticity coordinates and colour purity of GGTO:0.6Eu^{3+} under different temperatures.

Temperature (K)	CIE (*x*, *y*)	Colour purity (%)
300	(0.6484, 0.3512)	94.0
325	(0.6481, 0.3515)	93.9
350	(0.6478, 0.3518)	93.8
375	(0.6475, 0.3520)	93.7
400	(0.6467, 0.3528)	93.5
425	(0.6460, 0.3535)	93.4
450	(0.6450, 0.3545)	93.1
475	(0.6444, 0.3551)	93.0

Table S8. Judd-Ofelt studies on the photoluminescence data of the GGTO:0.6Eu^{3+} phosphor under different temperatures.

Temperature (K)	I_{01}	I_{02}	I_{02}/I_{01}	A_{02} (s^{-1})	Ω_2 ($\times 10^{-20}$ cm^2)
300	23181300	58590900	2.53	130.20	4.24
325	21378200	54433800	2.55	131.17	4.27
350	19746400	50531900	2.56	131.83	4.30
375	18125700	46684000	2.58	132.68	4.32
400	16132800	41574200	2.58	132.75	4.33
425	13821700	35760300	2.59	133.28	4.34
450	11170500	28948400	2.59	133.50	4.35
475	8087930	21286800	2.63	135.58	4.42

Table S9. The performance comparison of GGTO:0.6Eu^{3+} phosphor with some representative and recently reported Eu^{3+}-activated phosphors.

Phosphors	c_0 (%)	η (%)	$T_{400\ K}$ (%)	CP (%)	CRI	Ref.
$GdGaTi_2O_7:Eu^{3+}$	60	70.8	71	93.5	91.9	This work
$Ba_6Gd_2Ti_4O_{17}:Eu^{3+}$	100	24.0	47	94.4	82.2	1
$Cs_3GdGe_3O_9:Eu^{3+}$	100	94.0	>98	95.1	89.7	5
$Rb_2Ba_3(P_2O_7)_2:Eu^{3+}$	7	77.0	>87	96.4	72.8	6
$Sr_2LaNbO_6:Eu^{3+}$	30	33.5	71	94.6	86.9	7
$NaGdF_4:Eu^{3+}$	50	62.3	61	90.5	86.6	8
$NaTbF_4:Eu^{3+}$	30	50.2	73	89.2	91.9	9
$NaBiF_4:Eu^{3+}$	40	73.1	75	90.4	88.2	10
$Ca_2Gd_8Si_6O_{26}:Eu^{3+}$	30	53.9	71	93.8	84.8	11
$Y_2O_3:Eu^{3+}$	/	83.4	~76.0	/	/	12
$Y_2O_2S:Eu^{3+}$	/	68.7	~88.0	/	/	13,14
YVO4:Eu^{3+}	/	/	~70.0	/	/	15,16
$LaAlO_3$	/	~63.0	/	/	/	17

References

[1] J. Li, Q. Liang, Y. Cao, J. Yan, J. Zhou, Y. Xu, L. Dolgov, Y. Meng, J. Shi and M. Wu, Layered structure produced nonconcentration quenching in a novel Eu^{3+}-doped phosphor, *ACS Appl. Mater. Interfaces*, 2018, **10**, 41479-41486.

[2] C. Y. Peng, H. J. Zhang, J. B. Yu, Q. G. Meng, L. S. Fu, H. R. Li, L. N. Sun and X. M. Guo, Synthesis, characterization, and luminescence properties of the ternary europium complex covalently bonded to mesoporous SBA-15, *J. Phys. Chem. B*, 2005, **109**, 15278-15287.

[3] E. E. S. Teotonio, J. G. P. Espínola, H. F. Brito, O. L. Malta, S. F. Oliveira, D. L. A. Faria and C. M. S. Izumi, Influence of the N-[methylpyridyl]acetamide ligands on the photoluminescent properties of Eu(III)-perchloratecomplexes, *Polyhedron*, 2002, **21**, 1837-1844.

[4] Y. B. Hua, K. Hussain and J. S. Yu, Eu^{3+}-activated double perovskite Sr_3MoO_6 phosphors with excellent color purity for high CRI WLEDs and flexible display film, *J. Alloys Compd.*, 2019, **45**, 18604-18613.

[5] P. Dang, G. Li, X. Yun, Q. Zhang, D. Liu, H. Lian, M. Shang and J. Lin, Thermally stable and highly efficient red-emitting Eu^{3+}-doped $Cs_3GdGe_3O_9$ phosphors for WLEDs: non-concentration quenching and negative thermal expansion, *Light-Sci. & Appl.*, 2021, **10**, 29.

[6] C. Wang, Y. Li, S. Chen, Y. Li, Q. Lv, B. Shao, G. Zhu and L. Zhao, A novel high efficiency and ultra-stable red emitting europium doped pyrophosphate phosphor for multifunctional applications, *Inorg. Chem. Front.*, 2021, **8**, 3984-3997.

[7] Y. Hua, W. Ran and J. S. Yu, Excellent photoluminescence and cathodoluminescence properties in Eu^{3+}-activated Sr_2LaNbO_6 materials for multifunctional applications, *Chem. Eng. J.*, 2021, **406**, 127154.

[8] P. Du, W. Ran, Y. Hou, L. Luo and W. Li, Eu^{3+}-Activated $NaGdF_4$ nanorods for near-ultraviolet light-triggered indoor illumination, *ACS Appl. Nano Mater.*, 2019, **2**, 4275-4285.

[9] P. Du, W. Ran, W. Li, L. Luo and X. Huang, Morphology evolution of Eu^{3+}-activated $NaTbF_4$ nanorods: a highly-efficient near-ultraviolet light-triggered red-emitting platform towards application in white light-emitting diodes, *J. Mater. Chem. C*, 2019, **7**, 10802-10809.

[10] P. Du, X. Huang and J. S. Yu, Facile synthesis of bifunctional Eu^{3+}-activated $NaBiF_4$ red-emitting nanoparticles for simultaneous white light-emitting diodes and field emission displays, *Chem. Eng. J.*, 2018, **337**, 91-100.

[11] J. Du, X. Pan, Z. Liu, Y. Jing, B. Wang, L. Luo, J. Wang and P. Du, Highly efficient Eu^{3+}-activated $Ca_2Gd_8Si_6O_{26}$ red-emitting phosphors: A bifunctional platform towards white light-emitting diode and ratiometric optical thermometer applications, *J. Alloys Compd.*, 2021, **59**, 157843.

[12] Z. Chen, Y. Pan, L. Xi, R. Pang, S. Huang and G. Liu, Tunable yellow-red photoluminescence and persistent afterglow in phosphors $Ca_4LaO(BO_3)_3$:Eu^{3+} and $Ca_4EuO(BO_3)_3$, *Inorg. Chem.*, 2016, **55**, 11249−11257.

[13] Z. Sun, G. Cao, Q. Zhang, Y. Li and H. Wang, Thermal stable Eu-doped $CaTiO_3$ phosphors with morphology-control for high-power tricolor white LEDs. *Mater. Chem. Phys.*, 2012, **132**, 937-942.

[14] L. Wang, W. Guo, Y. Tian, P. Huang, Q. Shi and C. Cui, High luminescent brightness and thermal stability of red emitting $Li_3Ba_2Y_3(WO_4)_8$:Eu^{3+} phosphor, *Ceram. Int.*, 2016, **42**, 13648-13653.

[15] K. Riwotzki and M. Haase, Colloidal YVO_4:Eu and $YP_{0.95}V_{0.05}O_4$:Eu nanoparticles: luminescence and energy transfer processes, *J. Phys. Chem. B*, 2001, **105**, 12709-12713.

[16] G. Pan, H. Song, X. Bai, Z. Liu, H. Yu, W. Di, S. Li, L. Fan, X. Ren and S. Lu, Novel Energy-Transfer Route and Enhanced Luminescent Properties in YVO_4:Eu^{3+}/YBO_3:Eu^{3+} Composite, *Chem. Mater.*, 2006, **18**, 4526-4532.

[17] T. Manohar, R. Naik, S. C. Prashantha, H. Nagabhushana, S. C. Sharma, H. P. Nagaswarupa, K. S. Anantharaju, C. Pratapkumar and H.B. Premkumar,

Photoluminescence and Judd-Ofelt analysis of Eu^{3+} doped $LaAlO_3$ nanophosphors for WLEDs, *Dyes and Pigments*, 2015, **122**, 22-30.